

Microquasars: A Brief Overview and a Snapshot of GRS 1915+105 with *INTEGRAL*

D. C. Hannikainen¹ * and J. Rodriguez²

¹ Observatory, PO Box 14, FI-00014 University of Helsinki, Finland

² AIM – Astrophysique Interactions Multi-échelles (UMR 7158 CEA/CNRS/Université Paris 7 Denis Diderot), CEA Saclay, DSM/DAPNIA/Service d’Astrophysique, Bât. 709, l’Orme des Mesuriers, FR-91 191 Gif-sur-Yvette Cedex, France

Abstract Microquasars, sources of relativistic motion, have generated a lot of interest since their discovery. In this paper we shall briefly review some general properties of microquasars, and then focus on some recent observations of one of the more notorious microquasars, GRS 1915+105.

Key words: X-ray binaries — observations: X-ray — observations: radio — observations: γ -ray

1 MICROQUASARS

Quasars — supermassive black holes ($10^6 - 10^9 M_{\odot}$) accreting from their host galaxy — have been studied extensively since their discovery in the 1960s. One remarkable feature of these objects are the relativistic jets that emanate from the central source at apparent superluminal velocities, which were first observed in the radio.

1.1 X-ray Binaries

X-ray binaries consist of a compact object – either a neutron star or a black hole – feeding from a non-degenerate companion. The companion determines whether the X-ray binary is a high-mass or a low-mass X-ray binary – for high-mass X-ray binaries the companion is a massive OB star or a supergiant, whereas for low-mass X-ray binaries the companion is a lower main sequence star or a red giant. In both cases, the accretion of matter from the non-degenerate companion onto the compact object is the source of the X-ray emission. The accreted matter generally does not fall straight onto the surface of the neutron star or directly into the black hole, but forms an accretion disk around the compact object. This accretion disk is responsible for the soft X-ray ($\sim 2-10$ keV) emission. When there is a corona (i.e. a hot plasma cloud) surrounding the central compact object and the inner portions of the accretion disk, it can upscatter – via the inverse Compton process – the low energy photons to high energy photons (> 20 keV). Black hole X-ray binaries exist primarily in two different “states”: a high/soft state characterized by a strong disk blackbody component peaking at a few keV in X-ray spectra, accompanied by a weak powerlaw tail (sometimes with no observable cutoff up to the MeV range), and a low/hard state dominated by a powerlaw with a cutoff at ~ 100 keV interpreted as Comptonization by a population of thermalized electrons. Figure 1 shows Cygnus X-1 in the soft and in the hard state. There are other states, such as the intermediate, the very high, and the off states. The above is the “traditional” nomenclature for the states of black hole X-ray binaries that was in use until the late 1990s and even early 2000s. Recently, there have been several revisions in the taxonomy of states based on different criteria to those used traditionally, see e.g. McClintock & Remillard (2006) and Homan & Belloni (2005).

* E-mail: diana@astro.helsinki.fi

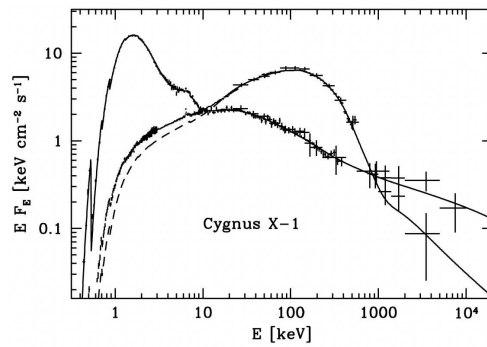


Fig. 1 Broadband spectra of Cygnus X-1. Note the soft state peaking at a few keV and the hard state with its cutoff. From McConnell et al. (2002).

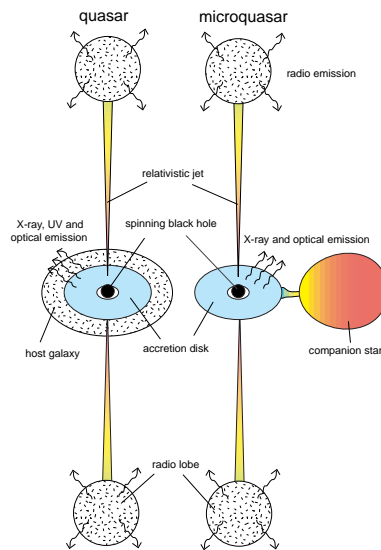


Fig. 2 A schematic illustration showing the similarity between microquasars and quasars (taken from Wu et al. 2002b).

It was the similarity in morphology between the extragalactic quasars and these radio-jet X-ray binaries — black hole, accretion disk, relativistic jets — that prompted the term “microquasars” for the latter (see Fig. 2).

1.2 Radio Jets

The first evidence that X-ray binaries may be sources of radio jets came when Spencer (1979), having observed SS433 in the radio, noted that the source was elongated. However, radio observations of X-ray binaries remained rather sparse until 1992 when Mirabel et al. (1992) using the Very Large Array observed a double-sided radio jet emanating from the Galactic Center source 1E1740.7–2942 (also known as the Great Annihilator). This prompted a flurry of activity in terms of radio observations. Then followed a remarkable observation, again with the Very Large Array, which revealed apparent superluminal ejections from the X-ray binary GRS 1915+105 (Mirabel & Rodríguez 1994). This was a first for a Galactic source. Once

corrected for relativistic effects, the true velocity of the ejecta was deemed to be $\sim 0.9c$ (this, of course, depends on the estimated distance to the object, which is a source of debate at the moment; see e.g. Chapuis & Corbel 2004; Kaiser et al. 2005).

There is an intimate relation between the source's X-ray activity and the birth of radio jets, prompting lively discussions on the exact connections between the accretion disk, the corona, and the jets themselves. (We will not discuss detailed X-ray:radio correlations in this paper, as it shall be dealt with elsewhere in these proceedings, see the contribution by Wilms). Originally, based on detailed *RXTE*/PCA observations of GRS 1915+105, it was assumed that the jets could be formed after the collapse of the inner portions of the accretion disk and that it was this material that was ejected away (e.g. Belloni et al. 1997). However, there are alternatives to this scenario, one of which is discussed below. What is indisputable, however, is that powerful jet ejection events usually occur following a state change in the X-ray binary which is manifested as major flaring in both soft and hard X-rays. See Fender, Belloni & Gallo (2004) for a detailed discussion on the role of state transitions and the formation of radio jets. Figure 3 shows an example of the soft and hard X-ray and radio lightcurves of XTE J1550–564 during its 1998 outburst. A powerful jet ejection event occurred right after the peak in the X-ray lightcurves, coincident with the peak in the radio lightcurve (Hannikainen et al. 2001).

2 A CLOSE LOOK AT GRS 1915+105 WITH INTEGRAL

2.1 GRS 1915+105

GRS 1915+105 has been extensively observed at all wavelengths ever since its discovery. It was originally detected as a hard X-ray source with the WATCH all-sky monitor on the *GRANAT* satellite (Castro-Tirado, Brandt & Lund 1992). Using the Very Large Telescope, Greiner et al. (2001) identified the mass-donating star to be of spectral type K-M III. The mass of the black hole was deduced by Harlaftis & Greiner (2004) to be $14.0 \pm 4.4 M_{\odot}$ in a binary orbit with the giant star of 33.5 days. In addition to the superluminal ejections at the arcsec scale mentioned above, GRS 1915+105 has also exhibited a compact radio jet resolved at milli-arcsec scales corresponding to a length of a few tens of AU (e.g. Fuchs et al. 2003). Belloni et al. (2000) categorized the variability into twelve distinct classes which they labelled with Greek letters (two of those represented by semi-regular pulsing behaviour), and identified three distinct X-ray states: two softer states, A and B, and a harder state, C (although note that GRS 1915+105 never really enters the canonical hard state).

2.2 INTEGRAL

The European Space Agency's INTERNATIONAL Gamma-Ray Astrophysical Laboratory (*INTEGRAL*) is aimed at observing the sky between ~ 3 keV and 10 MeV (Winkler et al. 2003). The *INTEGRAL* payload consists of two gamma-ray instruments – the Imager on Board the *INTEGRAL* Spacecraft, IBIS, and the Spectrometer on *INTEGRAL*, SPI; two identical X-ray monitors – the Joint European X-ray monitor, JEM-X of which only JEM-X1 is currently operational; and an optical monitor. Since *INTEGRAL*'s AO1 and our first observation of GRS 1915+105 in 2003 March (Hannikainen et al. 2003, 2005), we have consistently had a monitoring campaign on GRS 1915+105, although our strategy has altered slightly (later on we decided to perform shorter observations more frequently). The observations dealt with here are from 2004 October and November (AO2, revolutions 246 and 255), and for both we had supporting *RXTE* and radio observations (the Ryle and/or Nançay telescopes). They are from two different variability classes: revolution 246 is of class ν , while revolution 255 is class λ , according to the classification of Belloni et al. (2000).

2.3 Lightcurves

Figures 4 and 5 show the lightcurves and a zoom of the region of interest from Rev. 246 (ν) respectively, while Figures 6 and 7 show the same for Rev. 255 (λ). For full details on these observations and data reduction methods and analyses see Rodriguez et al. (2006, 2007a, b).

In both cases (Revs. 246 and 255) the JEM-X lightcurves show occurrences of soft X-ray dips of different duration, followed by a short spike marking the return to a high degree of soft X-ray emission and variability — we define this as a “cycle”. Also observed during both revolutions is a radio flare, indicative of the ejection of matter from the system. To further study the behavior of the source during these cycles, we

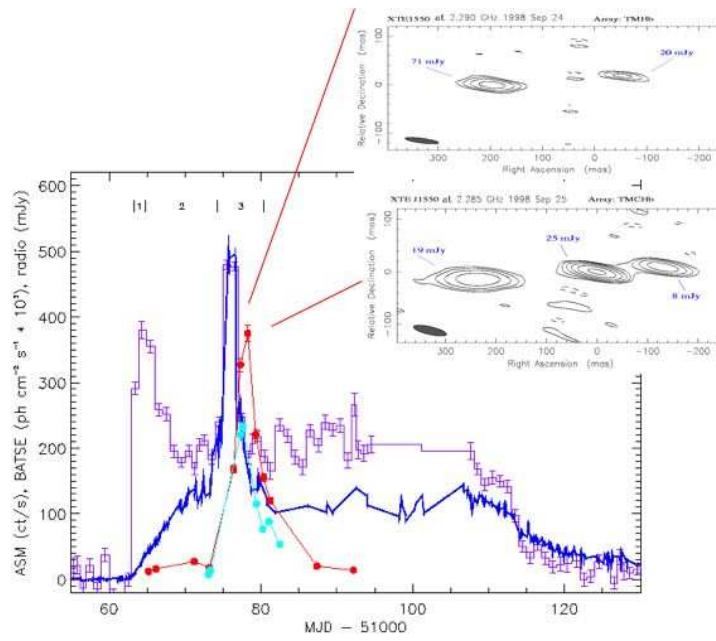


Fig. 3 The soft (*RXTE*/*ASM*, blue), hard (*BATSE*, purple) X-ray and radio (*ATCA*, cyan and *MOST*, red) lightcurves of XTE J1550–564 (from Wu et al. 2002a). Superposed are the *SHEVE* radio maps showing the evolution of the ejecta between 1998 Sept 24 and 1998 Sept 25 (from Hannikainen et al. 2001).

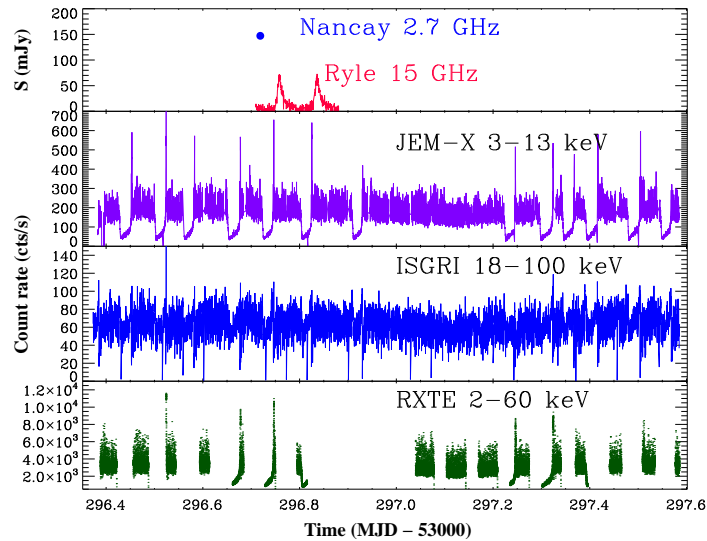


Fig. 4 Multiwavelength lightcurves of GRS 1915+105 representing two intervals of class ν from 2004 October. From top to bottom: the radio lightcurves (Ryle Telescope at 15 GHz in red, Nancay 2.7 GHz in blue); *JEM-X* 3–13 keV; *ISGRI* 18–100 keV; and *RXTE*/*PCA* 2–60 keV.

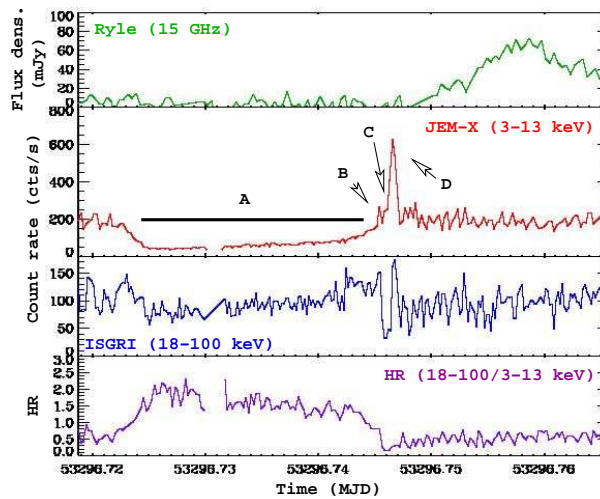


Fig. 5 A zoom of the area of interest. The letters correspond to the spectra in Fig. 8. Here, though, the bottom panel is the hardness ratio.

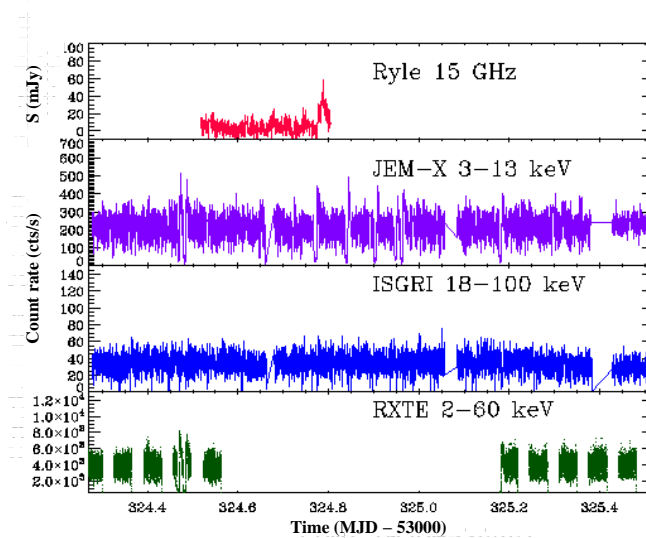


Fig. 6 The same as in Fig. 4 but for Rev. 255 representing class λ , although note that now there is no Nançay coverage.

subdivided the lightcurves into sections (labeled A, B, C and D in Figs. 5 and 7) from which we extracted spectra. This is dealt with in the next section.

2.4 Spectral Fitting

In a preliminary analysis, we separated the cycles from both revolutions (i.e. classes) into four distinct intervals: a soft X-ray dip (A), followed by a short precursor spike (B), a subsequent shorter dip (C) and a final main spike (D). We then studied the behavior of the accretion disk and that of the corona through the cycle. All spectra were fit with the same model: a thermal component described by `ezdiskbb` in XSPEC

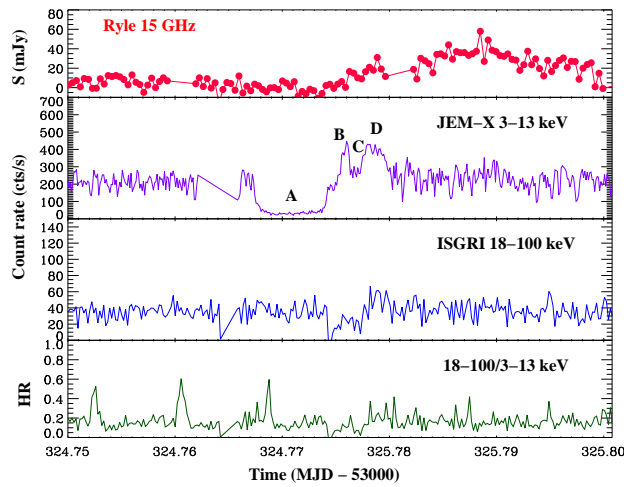


Fig. 7 A zoom of the area of interest. The letters correspond to the spectra in Fig. 9. The panels are the same as in Fig. 5.

and a Comptonized component described by `comptt`, modified by interstellar absorption which was fixed to $6 \times 10^{22} \text{ cm}^{-2}$. Interval A is characterized by a harder spectrum than intervals B, C, and D.

Figures 8 and 9 show the resulting spectra and their best-fit model, while the results of the parameters of the accretion disk are reported in Table 1. One can see that contrary to what was formerly supposed (e.g. Belloni et al. 1997), the disk approaches the black hole monotonically during the cycle. We then studied the evolution of the 3–50 keV flux from the individual components, i.e. the disk and the corona. Whereas the flux of the disk increases throughout the whole sequence, as expected from the evolution of its parameters, we see that the fluxes from the Comptonizing corona do not evolve in as simple a manner. In Rev. 246 (class ν), the corona flux first increases from interval A to interval B, followed by a reduction by a factor of 2.5 in interval C (to $F_{3-50\text{keV}} = 1.0 \times 10^{-8} \text{ erg cm}^{-2} \text{ s}^{-1}$), after which it slowly recovers in interval D ($F_{3-50\text{keV}} = 1.5 \times 10^{-8} \text{ erg cm}^{-2} \text{ s}^{-1}$). Similar behavior is observed in Rev. 255 (class λ), but now we see a reduction in the corona flux by a factor up to ~ 11 between intervals B and C (from $F_{3-50\text{keV}} = 2.2 \times 10^{-8} \text{ erg cm}^{-2} \text{ s}^{-1}$ to $F_{3-50\text{keV}} = 0.19 \times 10^{-8} \text{ erg cm}^{-2} \text{ s}^{-1}$, when allowing all the spectral parameters to vary). At interval D, the flux has again recovered slightly (to $F_{3-50\text{keV}} = 1.3 \times 10^{-8} \text{ erg cm}^{-2} \text{ s}^{-1}$). Note that a more refined analysis of the cycles is reported in Rodriguez et al. (2007b), and even though they could further divide the λ cycle (Rev. 255) into more intervals, the conclusions they reach are the same.

Table 1 Results from spectral fits to the intervals in Rev. 246 and 255

Interval	Rev. 246 (ν)		Rev. 255 (λ)	
	kT_{disk} (keV)	R_{in} (R_{g})	kT_{disk} (keV)	R_{in} (R_{g})
A	—	—	0.66	47
B	1.3	15.0	1.75	8.5
C	1.6	6.6	2.00	6.0
D	2.1	6.1	1.83	7.7

2.5 Results and Conclusions

In both cases, the evolution of the source through the cycles seems to be more pronounced in the soft X-rays. This would initially lead to the conclusion that the variations are caused by changes in the accretion

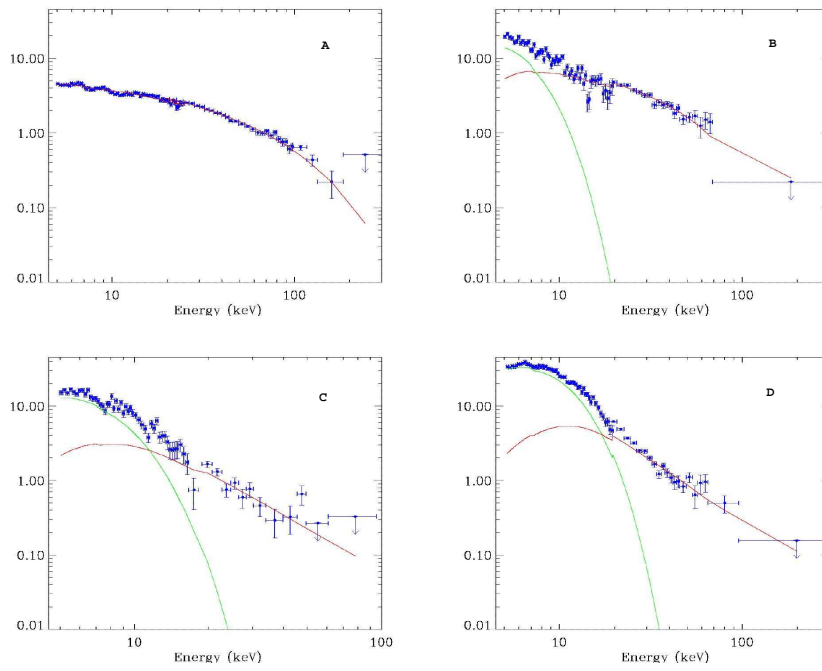


Fig. 8 The spectra from Rev. 246 (ν) with the best-fit models superimposed. The letters in the panels correspond to the intervals marked in Fig. 5. The green line represents the disk blackbody component, while the red line represents the Comptonized component.

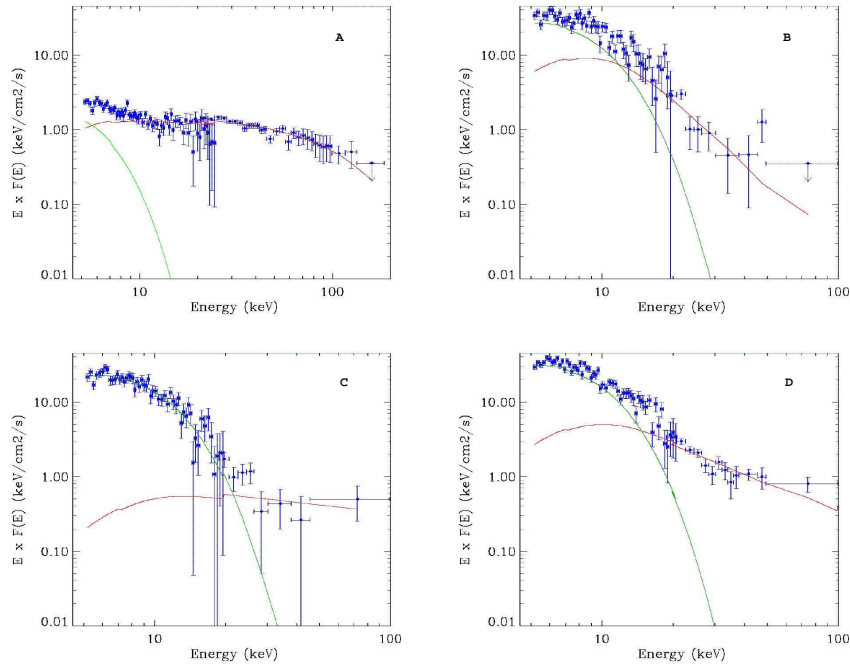


Fig. 9 The spectra from Rev. 255 (λ) with the best-fit models superimposed. The letters in the panels correspond to the intervals marked in Fig. 5. The green line represents the disk blackbody component, while the red line represents the Comptonized component.

disk, rather than in the Comptonized component. In both cases, we have seen that throughout the A-B-C-D sequences the inner radius of the accretion disk approaches the compact object monotonically, while the flux of the corona is greatly reduced between intervals B and C. The evolution through the intervals seems to be marked by a real change in the physical properties of the Comptonizing corona, which results in the spectral state change. This behavior suggests that the dip (C) following the precursor spike (B) is the result of the disappearance of the corona.

Considering we have the radio data showing a “reaction” to the cycle, we envision a scenario where the ejection occurs at the precursor spike (B) and therefore the ejected material (seen as the radio flare) is, in fact, the corona itself. It has already been shown that in class β , at least, the X-ray spike halfway through the dip is the trigger of the ejection (Mirabel et al. 1998). Chaty (1998) already suggested that during this particular class (β), the spike corresponds to the disappearance of the corona, hence it is the latter which makes up the ejecta. Rodriguez et al. (2002) also considered this scenario for class α in GRS 1915+105 and for the larger ejections witnessed from XTE J1550–564 (Rodriguez, Corbel & Tomsick 2003). The main difference between these two sources is the timescales on which these occur: in GRS 1915+105 these events occur several times per hour, whereas in XTE J1550–564 it is a single ejection event following the peak in the soft X-rays, but there is no reason to believe that they necessarily differ in mechanism.

Although we may be closer to answering the question regarding the exact moment of the ejection of material (and what that material may be) from the system, we are still far from understanding accretion-ejection mechanisms. What we can hope is that with our ongoing monitoring program of GRS 1915+105 we can gain a larger statistical database from which we can better determine the various contributions to the physical mechanisms which lead to ejection events in microquasars.

Acknowledgements DCH gratefully acknowledges a Fellowship from the Finnish Academy and a travel grant from the Magnus Ehrnrooth Foundation.

References

- Belloni T., Mendez M., King A. R., van der Klis M., van Paradijs J., 1997, *ApJ*, 488, L109
 Belloni T., Klein-Wolt M., Méndez M., van der Klis M., van Paradijs J., 2000, *A&A*, 355, 271
 Castro-Tirado A. J., Brandt S., Lund N., 1992, *IAUC*, 5590
 Chapuis C., Corbel S., 2004, *A&A*, 414, 659
 Chaty S., 1998, PhD thesis
 Fender R. P., Belloni T. M., Gallo E., 2004, *MNRAS*, 355, 1105
 Fuchs Y. et al., 2003, *A&A*, 409, L35
 Greiner J., Cuby J. G., McCaughrean M. J., Castro-Tirado A., Mennickent R. E., 2001, *A&A*, 373, L37
 Hannikainen D., Campbell-Wilson D., Hunstead R. et al., 2001, *Ap&SSS*, 276, 45
 Hannikainen D. C. et al., 2003, *A&A*, 411, L415
 Hannikainen D. C. et al., 2005, *A&A*, 435, 995
 Harlaftis E., Greiner J., 2004, *A&A*, 414, L13
 Homan J., Belloni T., 2005, *Ap&SS*, 300, 107
 Kaiser C. R., Sokoloski J. L., Gunn K. F., Brocksopp C., 2005, *Ap&SS*, 300, 283
 McClintock J. E., Remillard R. A., 2006, In: *Compact stellar X-ray sources*. Edited by Walter Lewin & Michiel van der Klis. Cambridge Astrophysics Series, No. 39. Cambridge, UK: Cambridge University Press, p.157
 McConnell M. L. et al., 2002, *ApJ*, 572, 984
 Mirabel I. F., Rodríguez L. F., Cordier B., Paul J., Lebrun F., 1992, *Nature*, 358, 215
 Mirabel I. F., Rodríguez L. F., 1994, *Nature*, 392, 673
 Mirabel I. F. et al., 1998, *A&A*, 330, L9
 Rodríguez J. et al., 2002, *A&A*, 386, 271
 Rodríguez J., Corbel S., Tomsick J., 2003, *ApJ*, 595, 1032
 Rodríguez J., Pooley G., Hannikainen D. et al., 2006, *Proceedings of the VI Microquasar Workshop: Microquasars and Beyond*, 24
 Rodríguez J. et al., 2008a, *ApJ*, 675, 1436
 Rodríguez J. et al., 2008b, *ApJ*, 675, 1449
 Spencer R., 1979, *Nature*, 282, 483
 Winkler C., Courvoisier T. J. -L., DiCocco G. et al., 2003, *A&A*, 411, L1
 Wu K. et al., 2002a, *ApJ*, 565, 1161
 Wu K., Stevens J. A., Hannikainen D. C., 2002b, *PASP*, 19, 91